ACS APPLIED MATERIALS & INTERFACES

Research Article

www.acsami.org

Facile and Mild Strategy to Construct Mesoporous CeO_2–CuO Nanorods with Enhanced Catalytic Activity toward CO Oxidation

Guozhu Chen,*[,†] Qihui Xu,[†] Ying Yang,[†] Cuncheng Li,[†] Taizhong Huang,[†] Guoxin Sun,[†] Shuxiang Zhang,[†] Dongling Ma,*[,‡] and Xu Li*[,§]

[†]Shandong Provincial Key Laboratory of Fluorine Chemistry and Chemical Materials, School of Chemistry and Chemical Engineering, University of Jinan, Jinan, Shandong 255022, China

[‡]Institut National de la Recherche Scientifique (INRS), 1650 Boulevard Lionel-Boulet, Varennes, Québec J3X 1S2, Canada

[§]Institute of Materials Research and Engineering, Agency for Science, Technology and Research (A*STAR), 3 Research Link, Singapore

Supporting Information

ABSTRACT: CeO_2–CuO nanorods with mesoporous structure were synthesized by a facile and mild strategy, which involves an interfacial reaction between $Ce_2(SO_4)_3$ precursor and NaOH ethanol solution at room temperature to obtain mesoporous CeO_2 nanorods, followed by a solvothermal treatment of as-prepared CeO_2 and $Cu(CH_3COO)_2$. Upon solvothermal treatment, CuO species is highly dispersed onto the CeO_2 nanorod surface to form CeO_2–CuO composites, which still maintain the mesoporous feature. A preliminary CO catalytic oxidation study demonstrated that the CeO_2–CuO samples exhibited strikingly high catalytic activity, and a high CO conversion rate was observed without obvious loss in activity even after thermal treatment at a high temperature of 500 °C. Raman spectroscopy, X-ray photoelectron spectroscopy (XPS), and hydrogen temperature-programmed reduction (H_2-TPR) analysis revealed that there is a strong interaction between CeO_2 and CuO. Moreover, it was found that the introduction of CuO species into CeO_2 generates oxygen vacancies, which is highly likely to be responsible for high catalytic activity toward CO oxidation of the mesoporous CeO_2–CuO nanorods.

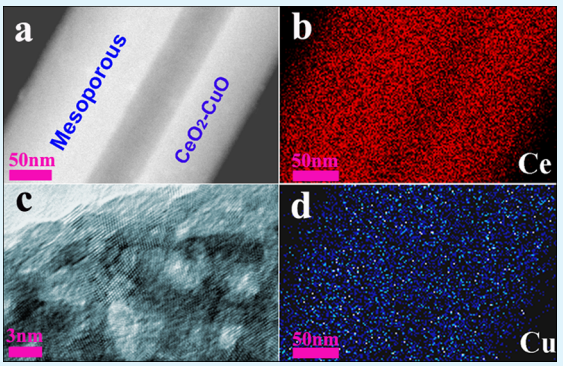

KEYWORDS: *ceria, interfacial reaction, bimetal oxide, composites, catalysis*

INTRODUCTION

Ceria has been widely studied as both catalyst and catalyst support for various reactions because of its unique properties, including excellent redox property and high oxygen storage capacity.[1−10] To enhance ceria catalytic activity, generally, one may either optimize its morphologies/structures or combine it with secondary species, for example, noble metals or other metal oxides, to form composites.[11−23] In the former strategy, various kinds of morphologies/structures of ceria have been designed and realized and its structure-dependent properties have been well studied as well.[7,12−14] Especially, the structure with high surface area, for example, a mesoporous structure, is highly desired since this kind of structure not only facilitates the dispersion of secondary components, but also enables reactant molecules to diffuse into the active sites easily.[8,15,16,24] In the latter strategy, although incorporated noble metals can significantly enhance the catalytic activity of ceria, their high price and limited resource hinder their practical applications to a certain extent. Alternatively, due to the synergistic effect, ceria-based bimetal oxides by combining ceria with other cheap transition metal oxides exhibit remarkable catalytic activity, which is even comparable to that of noble metal-based catalysts in some reactions.[19] Therefore, the construction of ceria-based bimetal oxides with high surface area could take full advantages of two strategies stated above, and thus is of particular interest to optimize their catalytic activities.

Among ceria-based bimetal oxides, CeO_2–CuO is one of most widely studied catalysts for CO oxidation, preferential oxidation, and water–gas shift owing to its high activity and good selectivity as well as low price.[19,25−34] Until now, precipitation,[27,28] impregnation,[29−32] and sol–gel[25,33] are commonly used methodologies to synthesize CeO_2–CuO catalysts. However, it is difficult to control morphology of the obtained catalysts, and furthermore, high temperature calcination is a necessary step in these methodologies. In addition, the obtained particles generally have a large size, low specific surface area and porosity. In order to increase the surface area of CeO_2–CuO composites, nanocasting has been employed. For example, Shi et al. prepared mesoporous CeO_2–CuO composites by a two-step approach, in which mesoporous

Received: July 17, 2015
Accepted: October 11, 2015
Published: October 11, 2015

DOI: 10.1021/acsami.5b06495
ACS Appl. Mater. Interfaces 2015, 7, 23538−23544

CeO_2 was first synthesized via nanocasting route followed by etching off silica KIT-6 hard template by NaOH solution, and then CuO was loaded into the CeO_2 through impregnation method.[32] In another case, Zhou et al. prepared mesoporous CeO_2−CuO composites by conanocasting technique, in which mixed Ce and Cu precursor solutions were coimpregnated into the mesoporous KIT-6 template, followed by calcination and template removal.[33] Although the nanocasting method provides a general and promising way in the synthesis of mesoporous materials, there are still remaining challenges with this strategy: the requirement of many synthesis steps, high temperature for calcination, and harsh conditions for template-removal process.

Porous/hollow CeO_2−CuO composites with high surface area can also be obtained through thermal decomposition of suitable precursors. For example, hollow CeO_2 was first obtained via calcination of $Ce(OH)CO_3$, which was prepared in the presence of acrylamide and ammonia under a hydrothermal condition for 72 h at 180 °C, and CuO was subsequently loaded by impregnation and calcination.[34] Hu et al. also prepared porous CeO_2−CuO composites through thermal decomposition of Ce−Cu binary precursor, which was synthesized from hydrothermal treatment of $Ce(NO_3)_3$, $Cu(NO_3)_2$, and urea mixed solution.[27] Recently, Zhang group synthesized porous CeO_2:Cu nanorods and nanobundles by means of calcination of Ce(Cu)-1,3,5 benzenetricarboxylic acid nanocrystals at 600 °C.[25] When porous CeO_2−CuO composites are derived from corresponding precursors, as stated in above examples,[25,27,34] the selection of precursors with designed structure becomes particularly important. An ideal precursor should (1) be easily prepared to simplify the whole preparation process, (2) be easily transformed into CeO_2−CuO, that is, avoiding calcination at high temperature, and (3) have a well-controlled morphology. Therefore, the development of novel precursors remains one of the hottest topics for construction of porous CeO_2-based binary metal oxides.

So far, various cerium-containing precursors, for example, Ce-alkoxide,[15] $Ce(OH)CO_3$,[35,36] and $Ce_2(C_2O_4)_3$,[37] are used to construct CeO_2 or CeO_2-based composites. For example, we have prepared Ce−Mn binary oxide nanotubes by the interfacial reaction between $Ce(OH)CO_3$ templates and $KMnO_4$ aqueous solution.[36] However, very little attention is paid to $Ce_2(SO_4)_3$ as a precursor, possibly due to its high decomposition temperature (up to 850 °C for transformation into CeO_2) and water-soluble characteristic. Recently, we synthesized hierarchically flowerlike CeO_2 by means of interfacial reaction between $Ce_2(SO_4)_3$ and NaOH, and demonstrated that the as-prepared CeO_2 is a good support for Au nanoparticles toward CO oxidation reaction in comparison to the CeO_2 derived from direct calcination of $Ce_2(SO_4)_3$.[38] The advantages of choosing water-soluble $Ce_2(SO_4)_3$ as precursor involve its easy preparation without the aid of surfactants, well-controlled morphology, and efficient transformation into CeO_2 without calcination. Furthermore, the residual $Ce_2(SO_4)_3$ can be washed away completely by water after interfacial reaction. Considering the advantages of one-dimensional structures and the synergistic effect in CeO_2-based bimetal oxide composites, herein, we choose $Ce_2(SO_4)_3$ nanorods as the precursor to synthesize mesoporous CeO_2−CuO bimetal oxide nanorods. The obtained CeO_2−CuO composites not only inherit initial rod-morphology of the $Ce_2(SO_4)_3$ precursor, but also generate mesoporous structure. Owing to the mesoporous structure, homogeneous dispersion of CuO, and close contact between CeO_2 and CuO, the as-prepared mesoporous CeO_2−CuO rods exhibit enhanced catalytic activity toward CO oxidation. Although the focus herein is on the CeO_2−CuO, we also demonstrate that this method can be easily extended to synthesize other mesoporous structures, such as Ce−Ni and Ce−Co oxide composites.

EXPERIMENTAL SECTION

Materials. Cerium(III) chloride heptahydrate ($CeCl_3·7H_2O$), copper(II) acetate monohydrate ($Cu(CH_3COO)_2·H_2O$), nickel(II) acetate tetrahydrate ($Ni(CH_3COO)_2·4H_2O$), cobalt(II) acetate tetrahydrate ($Co(CH_3COO)_2·4H_2O$), sodium hydroxide (NaOH), concentrated sulfuric acid (H_2SO_4), and ethanol were purchased from Sinopharm Chemical Reagent Co. Ltd. All the chemicals were of analytical grade and used as received without further purification.

Synthesis of $Ce_2(SO_4)_3$ Precursor. $Ce_2(SO_4)_3$ nanorods were prepared by mixing $CeCl_3·7H_2O$ and H_2SO_4 in ethanol. In a typical synthesis, 148 mg of $CeCl_3·7H_2O$ was first dissolved in 14.7 mL of anhydrous ethanol under vigorous magnetic stirring. Then, 1.3 mL of H_2SO_4 (0.75M) was added into the ethanol solution. The obtained white slurry was transferred into a Teflon-lined steel autoclave and heated for 3 h at 160 °C in an electric oven. Finally, the white product was collected by centrifugation and washed 3 times with absolute ethanol followed by drying at 80 °C overnight.

Synthesis of CeO_2. Mesoporous CeO_2 nanorods were prepared through the interfacial reaction between $Ce(SO_4)_3$ nanorods and NaOH. In a typical procedure, saturated NaOH ethanol solution was first prepared by dissolving NaOH into ethanol under ultrasonication and stirring for 1 h. Then 150 mg of as-prepared $Ce_2(SO_4)_3$ precursor was added into 30 mL of saturated NaOH ethanol solution and kept still for 2 days. Finally, the sample was washed with adequate ultrapure water 3 times followed by drying at 80 °C.

Synthesis of CeO_2−CuO. Different amounts of $Cu(CH_3COO)_2·H_2O$ were dissolved in 16 mL of ethanol under stirring. Then the as-prepared CeO_2 was added into the above clear green solutions under stirring. Subsequently, the obtained slurry was transferred into a Teflon-lined stainless steel autoclave and heated at 120 °C for 12 h. Finally, the sample was thoroughly washed with ultrapure water and dried at 80 °C.

Characterization. The phases and purity of the prepared samples were studied by X-ray powder diffraction (XRD) performed on a Rigaku D/Max-γA rotating anode X-ray diffractometer with Cu Kα radiation (λ = 1.54178 Å). N_2 adsorption−desorption isotherms were acquired using a Micromeritics ASAP 2020 surface area and pore size analyzer at 77 K. Before the measurement, the samples were outgassed in vacuum at 300 °C for 3 h. The surface areas were then estimated by the Brunauer−Emmett−Teller (BET) method, and the pore size distribution was calculated from the desorption branch using the Barrett−Joyner−Halenda (BJH) method. The morphology and structure of samples were studied by transmission electron microscopy (TEM; JEM 2100) and X-ray photoelectron spectrometer (XPS) with Al Kα radiation. The sample was dropped onto Au grid to analyze energy dispersive spectroscopy (EDS). Hydrogen temperature-programmed reduction (H_2-TPR) experiment was performed with a thermal conductivity detector on 50 mg sample in 80% (molar) argon and 20% (molar) hydrogen gas mixture, using a gas flow rate of 100 mL min^{-1} with a temperature ramp rate of 10 K min^{-1}. Micro-Raman measurements were taken with an LabRAM HR800 equipped with an excitation laser of 633 nm. The Cu contents in CeO_2−CuO samples were determined by inductively coupled plasma mass spectrometer (ICP-MS, Thermo Scientific XSeries-2).

Catalyst Test. Catalytic activity was studied using a continuous flow fixed-bed microreactor at atmospheric pressure. In a typical experiment, the system was first purged with high purity N_2 gas and then a gas mixture (1% CO, 10% O_2, 89% N_2) passed through the reactor at a flow rate of 50 mL/min, corresponding to a space velocity of 60 000 mL·h^{-1}·g^{-1} of catalyst. Composition of the gas exiting from the reactor was analyzed with an online infrared gas analyzer (Gasboard-3100, China Wuhan Cubic Co.), which can simultaneously detect CO, CO_2 and O_2.

DOI: 10.1021/acsami.5b06495
ACS Appl. Mater. Interfaces 2015, 7, 23538−23544

RESULTS AND DISCUSSION

Since $Ce_2(SO_4)_3$ is soluble in water, ethanol was chosen as reaction medium for the synthesis of CeO_2.[39] The phase purity and crystal structure of the synthesized samples were first examined by XRD. As shown in Figure 1, the $Ce_2(SO_4)_3$

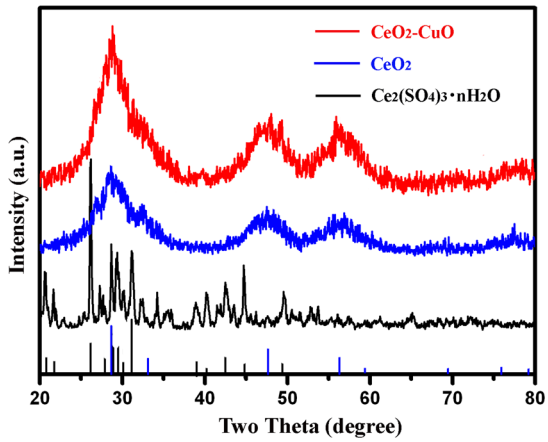

Figure 1. XRD patterns of $Ce_2(SO_4)_3$, CeO_2, and CeO_2−CuO (9 mol %) composites.

precursor mainly exists as orthorhombic $Ce_2(SO_4)_3{\cdot}nH_2O$ (JCPDS file no. 38-0572). In view of the great diversity of $Ce_2(SO_4)_3$ in hydrate number, other phases with different hydrate number possibly coexist.[40] After reaction at room temperature for 2 days, followed by a thorough water-washing step, the diffraction pattern of the sample can be well indexed as a pure, face-centered cubic phase of ceria (JCPDS no. 34-0394). It is reasonable that the residual $Ce_2(SO_4)_3$, if any, could be washed away by water during the sample purification process. Upon solvothermal reaction of the mixture of CeO_2 and $Cu(CH_3COO)_2$, no characteristic diffraction peaks of CuO were observed with the prepared sample. It indicates that either the CuO species is well dispersed onto the CeO_2 surface or/and copper is incorporated into the CeO_2 lattice. The broad diffraction peaks in both CeO_2 and CeO_2−CuO samples reveal their small crystalline size. Following the Scherrer equation, CeO_2 and CeO_2−CuO samples were found to show similar crystallite size, which is 2.9 nm for CeO_2 and 3.1 nm for CeO_2−CuO.

The morphology of the samples was investigated by TEM. Figure 2a shows that the as-synthesized $Ce_2(SO_4)_3$ precursor is characteristic of one-dimensional rod structure. After the $Ce_2(SO_4)_3$ precursor was treated with NaOH in ethanol, most of the synthesized CeO_2 nanostructures still maintain the rod morphology of the precursor. But interestingly, porous characteristic can now be clearly identified in these nanorods (Figure 2b). After further reaction between CeO_2 and $Cu(CH_3COO)_2$ at 160 °C, the obtained CeO_2−CuO composites still keep the rod morphology with porous structure without any obvious disturbance from severe solvothermal treatment (Figure 2c-f). Some pores spread over the rod, as shown in Figure 2e, f. The lattice fringes are clearly visible with spacing of 0.31 nm and the measured interplanar angle of around 70.5°, corresponding to the {111} crystal planes of ceria (Figure 2f).

To further investigate the elemental distribution of Ce and Cu in the porous nanorods, high angle annular dark field (HAADF)-scanning transmission electron microscopy (STEM)

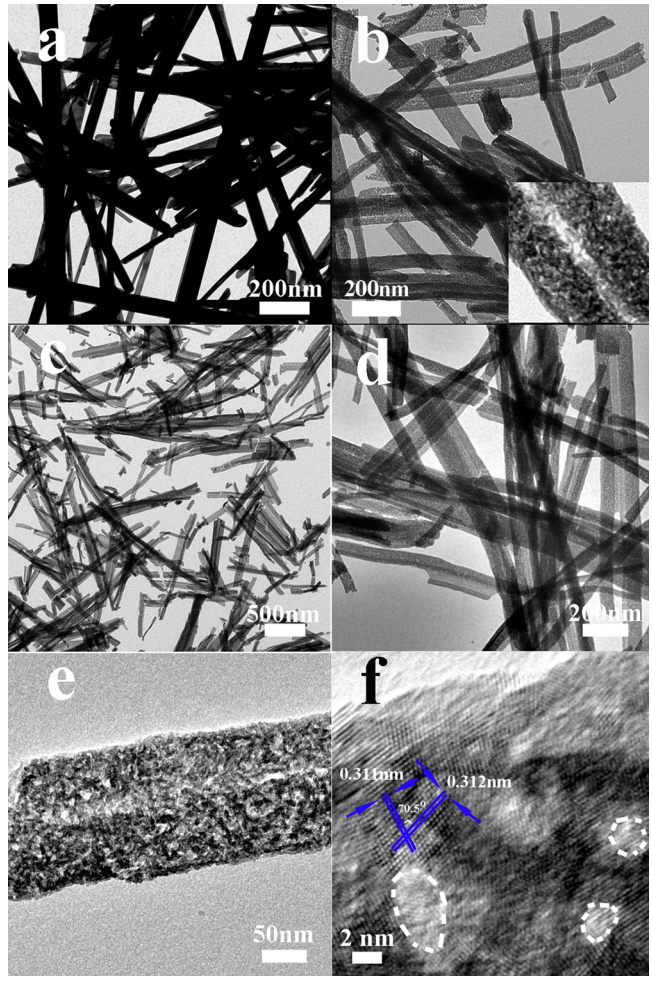

Figure 2. TEM images of (a) $Ce_2(SO_4)_3$, (b) CeO_2, and (c−f) CeO_2−CuO (9 mol %) with different magnifications. Some mesopores are outlined by white dashed lines in (f). Inset in (b) is the magnified image of CeO_2 porous nanorod.

image and elemental maps of an individual rod are collected. As shown in Figure 3, Ce, Cu, and O are uniformly distributed in the whole porous nanorod. This kind of uniform elemental distribution is absolutely favorable for the interaction between CeO_2 and CuO.

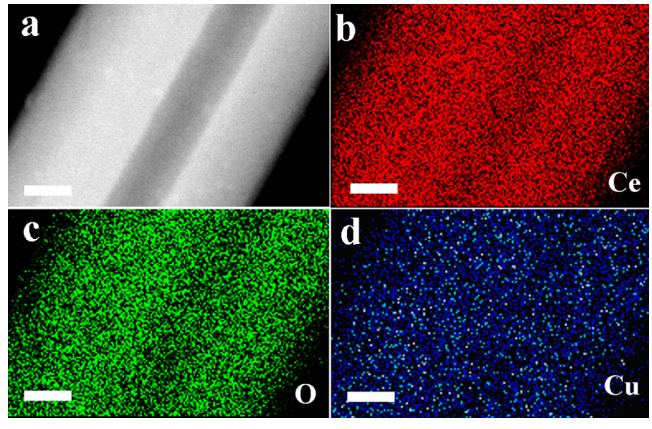

Figure 3. HAADF-STEM image (a), and Ce (b), O (c), and Cu (d) STEM-EDX maps of an individual CeO_2−CuO (9 mol %) rod. Scale bar: 50 nm.

DOI: 10.1021/acsami.5b06495
ACS Appl. Mater. Interfaces 2015, 7, 23538−23544

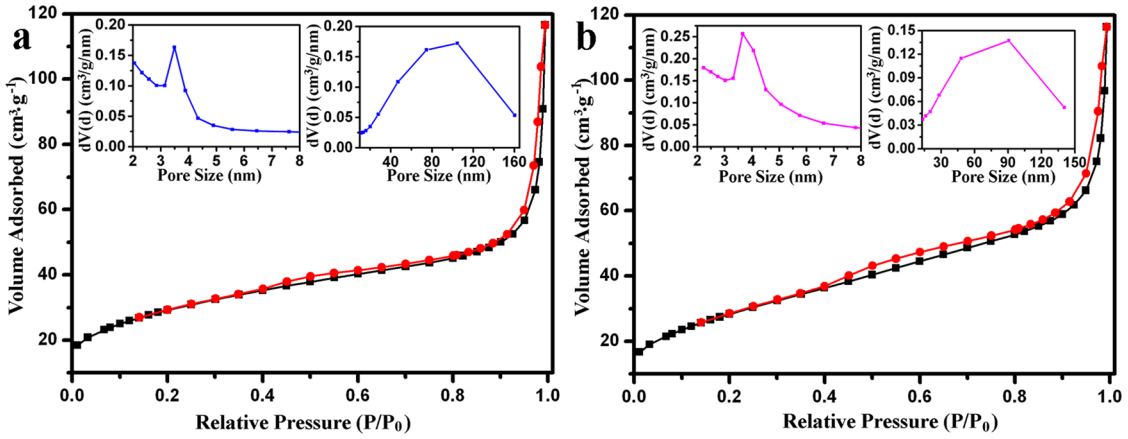

Figure 4. Nitrogen adsorption−desorption isotherms and corresponding BJH pore size distributions (insets) for the CeO_2 (a) and CeO_2−CuO (9 mol %) composite (b).

The nitrogen adsorption−desorption isotherms of CeO_2 and CeO_2−CuO composites exhibit the type-H3 hysteresis loop that is characteristic of mesoporous materials (Figure 4). The measured BET areas are around ∼105 $m^2\ g^{-1}$ for CeO_2 and ∼104 $m^2\ g^{-1}$ for CeO_2−CuO. The corresponding pore size distribution curves, determined from the desorption branches using the BJH method, are shown in the insets in Figure 4. They clearly confirm that both of the CeO_2 and CeO_2−CuO samples show bimodal size distributions of pores, which are composed of the mesopores of ∼3.5 nm in diameter and large voids ranging from 20 to 160 nm. The significant increase in surface area of CeO_2, compared with that of $Ce_2(SO_4)_3$ (∼7.4 $m^2\ g^{-1}$) (Figure S1), further implies generation of mesopores within CeO_2, which is consistent with the TEM results.

Since hydrated $Ce_2(SO_4)_3$ has a chain structure by the edge sharing of cerium polyhedra that are held together by sulfate group,[39] the $Ce_2(SO_4)_3$ prepared by mixing $CeCl_3$ and H_2SO_4 could develop into rod morphology under solvothermal conditions. Upon the addition of $Ce_2(SO_4)_3$ nanorods into NaOH ethanol solution, there is a liquid−solid interface reaction between the $Ce_2(SO_4)_3$ and OH^-. The Ce^{3+} ions slowly dissociated from $Ce_2(SO_4)_3$ react with OH^- to generate $Ce(OH)_3$, which is easily converted into CeO_2 through oxidation-dehydration during the drying process. The decrease in density from $Ce_2(SO_4)_3$ to CeO_2 and the loss of crystal water from $Ce_2(SO_4)_3$ precursor are possibly responsible for the generation of pores in CeO_2.[38] A little amount of residual $Ce_2(SO_4)_3$ precursor, mainly located at central part of rods, would be removed during the purification process by water, creating hollows in those rods (Figure 2b and Figure S2). During the second solvothermal process, alcoholysis of $Cu(CH_3COO)_2$ produces $Cu(OH)_2$ on the surface of CeO_2, followed by decomposition of $Cu(OH)_2$ into CuO. The formation mechanism is illustrated in Scheme 1. When $Ce_2(SO_4)_3$ nanorods were directly mixed with $Cu(CH_3COO)_2$ under the same experimental conditions, separate, spherical CuO nanoparticles with the average diameter of ∼50 nm were obtained instead of the rod structure (Figure 5a). XRD analysis

Scheme 1. Schematic Illustration of Formation of CeO_2−CuO Mesoporous Structured Materials

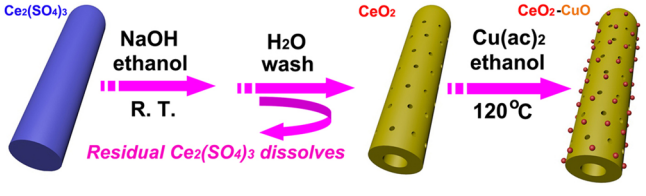

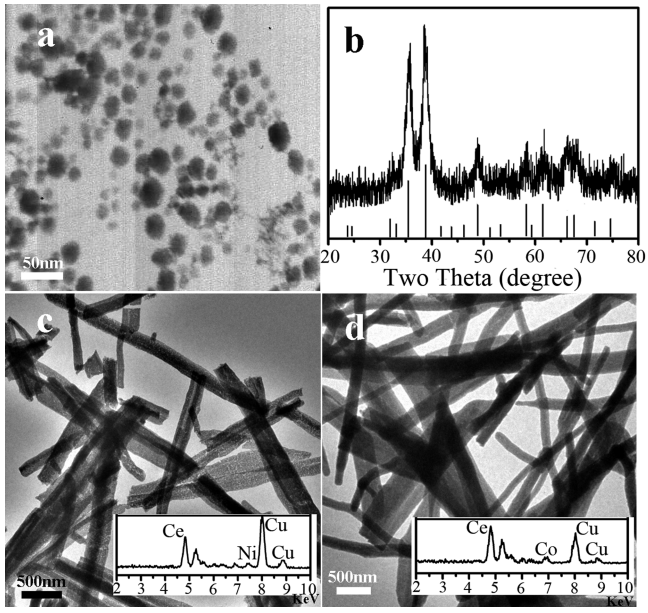

Figure 5. TEM image (a) and XRD pattern of CuO (b). TEM images of Ce−Ni (c) and Ce−Co (d) composites. Insets in (c) and (d) are corresponding EDS patterns.

indicates that the product is crystalline CuO with monoclinic phase (JCPDS file no. 44-0706) (Figure 5b). These results demonstrate that the well dispersion of CuO onto mesoporous CeO_2 surface could be ascribed to hydroxyl groups on the CeO_2 surface, which easily interact with $Cu(OH)_2$ nuclei through hydrogen bond. Using the same approach, mesoporous Ce−Ni and Ce−Co oxide composites were synthesized when mesoporous CeO_2 rods were mixed with $Ni(CH_3COO)_2$ or $Co(CH_3COO)_2$, where pores were once again observed in TEM images (Figure 5c, d) and both Ce and Ni or Ce and Co elements coexist in the selected rods (insets in Figure 5c, d). These results demonstrate the importance of formation of the porous CeO_2 nanorods and the universality of this strategy in the synthesis of mesoporous binary metal oxide nanorods.

DOI: 10.1021/acsami.5b06495
ACS Appl. Mater. Interfaces 2015, 7, 23538−23544

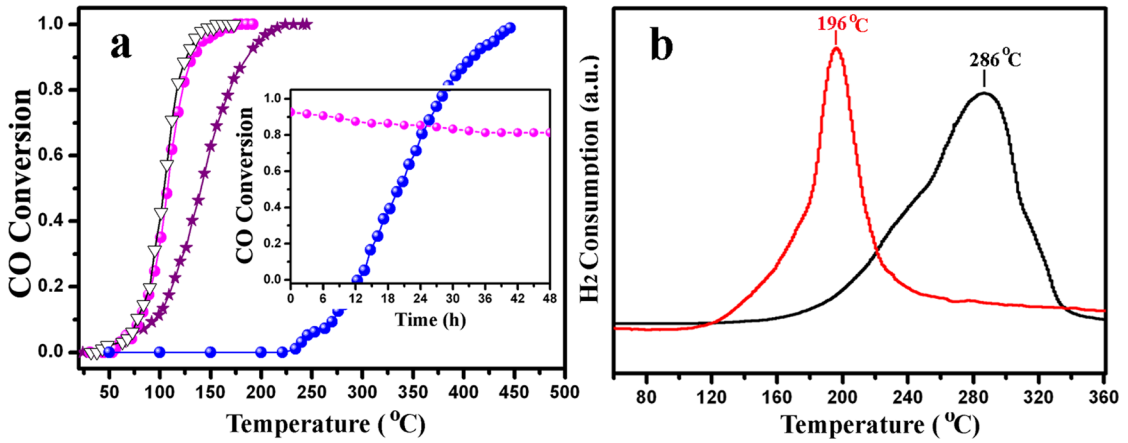

Figure 6. (a) CO conversion as a function of temperature for mesoporous CeO_2 (blue sphere), CeO_2−CuO (5.6 mol %) (purple star), CeO_2−CuO (9 mol %) (pink sphere), and CeO_2−CuO (14.1 mol %) (white triangle). Inset in (a) is the stability testing of CeO_2−CuO (9 mol %) catalyst at 120 °C for catalytic oxidation under the conditions of (a). (b) H_2-TPR profiles of CeO_2−CuO (9 mol %) sample (red line) and pure CuO (black line).

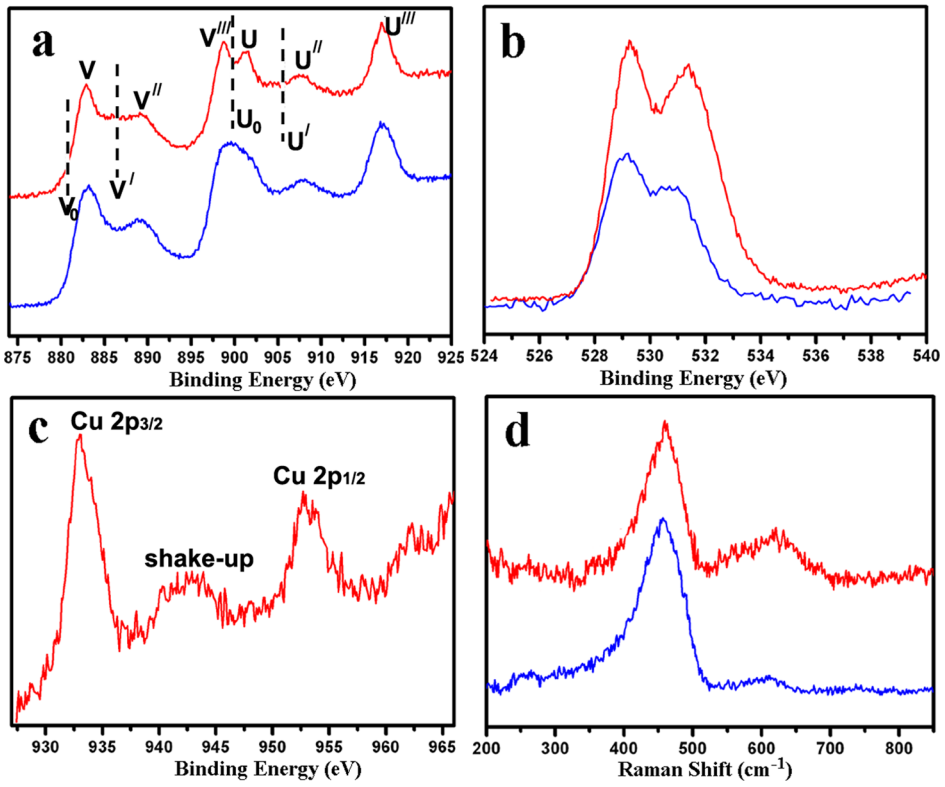

Figure 7. XPS spectra of (a) Ce 3d, (b) O 1s, (c) Cu 2p, and (d) Raman spectra of CeO_2 and CeO_2−CuO (9 mol %) composites. Blue curves refer to CeO_2, and red ones refer to CeO_2−CuO.

As aforementioned, CeO_2−CuO composites are being used in many catalytic reactions.[25−34] Herein, CO catalytic oxidation, being a model reaction, was carried out to evaluate the catalytic performance of the obtained CeO_2−CuO nanorods with different Cu contents and porous CeO_2 for comparison. Their light-off curves for CO oxidation are presented in Figure 6a. Since mesoporous CeO_2 has a similar physical feature to that of CeO_2−CuO, for example, surface area, pore size, and pore volume (Table S1), the enhanced catalytic activity of CeO_2−CuO must be due to the incorporation of CuO into porous CeO_2 instead of their difference in physical features. Specifically, when 5.6 mol % CuO was introduced, T_{50} (temperature at which 50% CO conversion has been achieved) decreased to ∼139 °C, in contrast to ∼336 °C for porous CeO_2. With further increase of CuO content to 9 and 14.1 mol %, even higher catalytic activity was achieved, with their T_{50} decreasing to ∼104 and ∼101 °C, respectively. The stability of catalyst is another important performance indicator. To study the durability of the mesoporous catalyst, the CeO_2−CuO (9 mol %) sample was selected as a typical example and CO oxidation reaction was continuously carried out for 48 h. As shown in the inset of Figure 6a, CO oxidation of 81% could still be achieved with only ∼10% of decrease in the catalytic activity in comparison with initial conversion at 120 °C. To study the thermal stability of the CeO_2−CuO catalyst, the sample was precalcined at 500 °C for 2 h. As shown in Figure S3, the

DOI: 10.1021/acsami.5b06495
ACS Appl. Mater. Interfaces 2015, 7, 23538−23544

calcined sample essentially maintained the high catalytic activity and complete CO oxidation was observed at 160 °C, although the sample surface became rougher and crystallite size increased (Figure S3 inset and Figure S4).

The CO oxidation reaction is dependent on the redox properties of catalysts. Herein, H_2-TPR analysis was performed to gain the information about the reducibility and the chemical state of copper species of the as-prepared CeO_2−CuO (9 mol %) composite. In general, a H_2 consumption peak centered at around 300 °C was observed in the pure CuO sample that was synthesized using a conventional precipitation method, while two peaks located approximately at 450 and 850 °C were observed for the pure CeO_2 sample.[26,33] As shown in Figure 6b, the H_2-TPR reduction peak of CeO_2−CuO (9 mol %) composite is located at ∼196 °C, which can be attributed to the reduction of the highly dispersed, small sized CuO species. Compared with the reduction of pure CuO (∼286 °C), the decrease in the reduction temperature of CuO in the prepared CeO_2−CuO composite reveals the strong interaction between the CuO species and the CeO_2.[28,31]

In order to illuminate the surface composition of as-prepared samples and to acquire detailed information on the chemical states of the related components, XPS was performed. As shown in Figure 7a, for the Ce 3d spectrum, both samples exhibit similar profiles where the six peaks marked as v, $v^{//}$, $v^{///}$, u, $u^{//}$, and $u^{///}$ are associated with Ce(IV), while the four peaks marked as v_0, $v^{/}$, u_0, and $u^{/}$ correspond to Ce(III).[15,28,31] In addition, the XPS O 1s spectra for the CeO_2 and CeO_2−CuO were also examined (Figure 7b). In general, the main peak in the range of 529−530 eV can be indexed to the lattice oxygen and the peak located at high binding energy ranging from 531 to 532.8 eV is assigned to defective or adsorptive oxygen species in CeO_2. With the stronger O_β peak, the CeO_2−CuO is expected to have a better capacity for oxygen storage.[26] In addition, the peak at 933−934.2 eV in combination with the appearance of a shakeup peak, characteristics of Cu $2p_{3/2}$, and the peak at 952.5−953.3 eV, characteristics of Cu $2p_{1/2}$ were observed, indicating that Cu mainly exists as Cu(II) in the CeO_2−CuO sample (Figure 7c). This sample was further studied by performing Raman spectroscopy measurements. As shown in Figure 7d, the peak centered at ∼458 cm^{-1} is assigned to the F_{2g} Raman active mode of cubic-phase CeO_2, corresponding to the symmetric breathing mode of oxygen atoms around cerium ions. However, a relatively high intensity, broad band between 550 and 650 cm^{-1}, which is commonly related to the presence of oxygen vacancies,[26,29,30] is clearly present in the Raman spectrum of the CeO_2−CuO sample compared to that of the CeO_2. This observation demonstrates the presence of increased number of oxygen vacancies in the composite sample.

During CO catalytic oxidation, it is widely accepted that the whole process mainly involves the adsorption and desorption of gas molecules on the surface/or at the interface of the catalyst. In the case of CeO_2−CuO, the incorporation of CuO species into CeO_2 could largely promote the creation of oxygen vacancies at or around the CeO_2−CuO interface in the presence of an appropriate amount of CuO, if any CuO enters the lattice of CeO_2, or there is strong interaction between CuO and CeO_2 across the interface.[26,27] In turn, the oxygen vacancies increase the adsorption amount and capacity of CeO_2−CuO for oxygen molecules, and promote the dissociation of O_2 into O_{ads}, thus facilitating the CO oxidation.[26,33] The number of oxygen vacancies will increase with increasing Cu doping, which in principle leads to higher catalytic activity of CeO_2−CuO sample. However, an excessive amount of CuO doped into CeO_2 may block the pore channel and cover the active sites of CeO_2, consequently, resulting in reduced catalytic activity.[19]

CONCLUSIONS

In summary, mesoporous CeO_2−CuO binary oxide nanorods were successfully fabricated by an interfacial reaction between $Ce_2(SO_4)_3$ nanorods and NaOH in ethanol, followed by a solvothermal process with $Cu(CH_3COO)_2$. The advantages of choosing $Ce_2(SO_4)_3$ as precursor include its easy preparation, well-controlled morphology, and efficient transformation into CeO_2 without calcination. More importantly, the transformation from $Ce_2(SO_4)_3$ into CeO_2 enables the formed CeO_2 and CeO_2−CuO mesoporous structures keeping initial rod morphology. Meanwhile, the as-prepared mesoporous CeO_2−CuO nanorods display enhanced catalytic activity toward CO oxidation. This work also provides a simple approach for preparing porous binary metal oxide materials with an interesting mesoporous structure from water-soluble precursors by means of the interfacial reaction.

ASSOCIATED CONTENT

Supporting Information

The Supporting Information is available free of charge on the ACS Publications website at DOI: 10.1021/acsami.5b06495.

TEM images, XRD pattern and catalytic activity of CeO_2−CuO (9 mol %) that was pretreated at 500 °C for 2 h, surface area, pore size, and pore volume data of $Ce_2(SO_4)_3$ and CuO, TEM image of the sample achieved from 2 day interfacial reaction between $Ce_2(SO_4)_3$ and NaOH in ethanol before water washing (PDF)

AUTHOR INFORMATION

Corresponding Authors

*E-mail: chm_chengz@ujn.edu.cn.
*E-mail: ma@emt.inrs.ca.
*E-mail: x-li@imre.a-star.edu.sg.

Notes

The authors declare no competing financial interest.

ACKNOWLEDGMENTS

This work is supported by the Shandong Provincial Natural Science Foundation, China (Grant no. ZR2015BM008), National Natural Science Foundation of China (Grant no. 21103068, 21171069), Science Development Project of Shandong Provincial 2014GGX104004.

REFERENCES

(1) Li, X.; Wang, X.; Liu, D.; Song, S.; Zhang, H. Multifunctional Nanostructures Based on Porous Silica Covered Fe_3O_4@CeO_2-Pt Composites: A Thermally Stable and Magnetically-Recyclable Catalyst System. *Chem. Commun.* **2014**, *50*, 7198−7201.

(2) Wang, F.; Wang, X.; Liu, D.; Zhen, J.; Li, J.; Wang, Y.; Zhang, H. High-Performance $ZnCo_2O_4$@CeO_2 Core@Shell Microspheres for Catalytic CO Oxidation. *ACS Appl. Mater. Interfaces* **2014**, *6*, 22216−22223.

(3) Ke, J.; Xiao, J. W.; Zhu, W.; Liu, H.; Si, R.; Zhang, Y. W.; Yan, C. H. Dopant-Induced Modification of Active Site Structure and Surface Bonding Mode for High-Performance Nanocatalysts: CO Oxidation on Capping-free (110)-oriented CeO_2:Ln (Ln = La-Lu) Nanowires. *J. Am. Chem. Soc.* **2013**, *135*, 15191−15200.

DOI: 10.1021/acsami.5b06495
ACS Appl. Mater. Interfaces 2015, 7, 23538−23544

(4) Qi, J.; Chen, J.; Li, G.; Li, S.; Gao, Y.; Tang, Z. Facile Synthesis of Core-Shell Au@CeO_2 Nanocomposites with Remarkably Enhanced Catalytic Activity for CO Oxidation. *Energy Environ. Sci.* **2012**, *5*, 8937−8941.
(5) Sreeremya, T. S.; Krishnan, A.; Remani, K. C.; Patil, K. R.; Brougham, D. F.; Ghosh, S. Shape-Selective Oriented Cerium Oxide Nanocrystals Permit Assessment of the Effect of the Exposed Facets on Catalytic Activity and Oxygen Storage Capacity. *ACS Appl. Mater. Interfaces* **2015**, *7*, 8545−8555.
(6) Li, H.; Lu, G.; Dai, Q.; Wang, Y.; Guo, Y.; Guo, Y. Hierarchical Organization and Catalytic Activity of High-Surface-Area Mesoporous Ceria Microspheres Prepared Via Hydrothermal Routes. *ACS Appl. Mater. Interfaces* **2010**, *2*, 838−846.
(7) Si, R.; Flytzani-Stephanopoulos, M. Shape and Crystal-Plane Effects of Nanoscale Ceria on the Activity of Au-CeO_2 Catalysts for the Water-Gas Shift Reaction. *Angew. Chem.* **2008**, *120*, 2926−2929.
(8) Liu, B.; Yu, S.; Wang, Q.; Hu, W.; Jing, P.; Liu, Y.; Jia, W.; Liu, Y.; Liu, L.; Zhang, J. Hollow Mesoporous Ceria Nanoreactors with Enhanced Activity and Stability for Catalytic Application. *Chem. Commun.* **2013**, *49*, 3757−3759.
(9) Jin, C.; Cao, X.; Lu, F.; Yang, Z.; Yang, R. Facile Synthesis of Gold-Nanoparticle-Decorated $Gd_{0.3}Ce_{0.7}O_{1.9}$ Nanotubes with Enhanced Catalytic Activity for Oxygen Reduction Reaction. *ACS Appl. Mater. Interfaces* **2014**, *6*, 847−853.
(10) Gao, Y.; Wang, W.; Chang, S.; Huang, W. Morphology Effect of CeO_2 Support in the Preparation, Metal-Support Interaction, and Catalytic Performance of Pt/CeO_2 Catalysts. *ChemCatChem* **2013**, *5*, 3610−3620.
(11) Song, S.; Wang, X.; Zhang, H. J. CeO_2-Encapsulated Noble Metal Nanocatalysts: Enhanced Activity and Stability for Catalytic Application. *NPG Asia Mater.* **2015**, *7*, 179−197.
(12) Huang, X. S.; Sun, H.; Wang, L. C.; Liu, Y. M.; Fan, K. N.; Cao, Y. Morphology Effects of Nanoscale Ceria on the Activity of Au/CeO_2 Catalysts for Low-Temperature CO Oxidation. *Appl. Catal., B* **2009**, *90*, 224−232.
(13) Sun, W.; Li, H.; Chen, L. Nanostructured Ceria-Based Materials: Synthesis, Properties, and Applications. *Energy Environ. Sci.* **2012**, *5*, 8475−8505.
(14) Liu, L.; Yao, Z.; Deng, Y.; Gao, F.; Liu, B.; Dong, L. Morphology and Crystal-Plane Effects of Nanoscale Ceria on the Activity of CuO/CeO_2 for NO Reduction by CO. *ChemCatChem* **2011**, *3*, 978−989.
(15) Zhong, L. S.; Hu, J. S.; Cao, A. M.; Liu, Q.; Song, W. G.; Wan, L. J. 3D Flowerlike Ceria Micro/Nanocomposite Structure and Its Application for Water Treatment and CO Removal. *Chem. Mater.* **2007**, *19*, 1648−1655.
(16) Li, G.; Li, L.; Jiang, D.; Li, Y.; Shi, J. One-Pot Synthesis of Meso-Structured Pd-CeO_x Catalyst for Efficient Low-Temperature CO Oxidation under Ambient Conditions. *Nanoscale* **2015**, *7*, 5691−5698.
(17) An, K.; Alayoglu, S.; Musselwhite, N.; Plamthottam, S.; Melaet, G.; Lindeman, A. E.; Somorjai, G. A. Enhanced CO Oxidation Rates at the Interface of Mesoporous Oxides and Pt Nanoparticles. *J. Am. Chem. Soc.* **2013**, *135*, 16689−16696.
(18) Cui, J.; Zhang, X.; Tong, L.; Luo, J.; Wang, Y.; Zhang, Y.; Xie, K.; Wu, Y. A Facile Synthesis of Mesoporous Co_3O_4/CeO_2 Hybrid Nanowire Arrays for High Performance Supercapacitors. *J. Mater. Chem. A* **2015**, *3*, 10425−10431.
(19) Shi, J. On the Synergetic Catalytic Effect in Heterogeneous Nanocomposite Catalysts. *Chem. Rev.* **2013**, *113*, 2139−2181.
(20) Yang, J.; Lukashuk, L.; Akbarzadeh, J.; Stöger-Pollach, M.; Peterlik, H.; Föttinger, K.; Rupprechter, G.; Schubert, U. Different Synthesis Protocols for Co_3O_4-CeO_2 Catalysts-Part 1: Influence on the Morphology on the Nanoscale. *Chem. - Eur. J.* **2015**, *21*, 885−892.
(21) Cui, X.; Wang, Y.; Chen, L.; Shi, J. Synergetic Catalytic Effects in Tri-Component Mesostructured Ru-Cu-Ce Oxide Nanocomposite in CO Oxidation. *ChemCatChem* **2014**, *6*, 2860−2871.
(22) Zhen, J.; Wang, X.; Liu, D.; Song, S.; Wang, Z.; Wang, Y.; Li, J.; Wang, F.; Zhang, H. Co_3O_4 @CeO_2 Core@Shell Cubes: Designed Synthesis and Optimization of Catalytic Properties. *Chem. - Eur. J.* **2014**, *20*, 4469−4473.
(23) Ta, N.; Liu, J.; Chenna, S.; Crozier, P. A.; Li, Y.; Chen, A.; Shen, W. Stabilized Gold Nanoparticles on Ceria Nanorods by Strong Interfacial Anchoring. *J. Am. Chem. Soc.* **2012**, *134*, 20585−20588.
(24) Jin, R.; Yang, Y.; Xing, Y.; Chen, L.; Song, S.; Jin, R. Facile Synthesis and Properties of Hierarchical Double-Walled Copper Silicate Hollow Nanofibers Assembled by Nanotubes. *ACS Nano* **2014**, *8*, 3664−3670.
(25) Li, S.; Wang, N.; Yue, Y.; Wang, G.; Zu, Z.; Zhang, Y. Copper Doped Ceria Porous Nanostructures towards a Highly Efficient Bifunctional Catalyst for Carbon Monoxide and Nitric Oxide Elimination. *Chem. Sci.* **2015**, *6*, 2495−2500.
(26) Yang, F.; Wei, J.; Liu, W.; Guo, J.; Yang, Y. Copper Doped Ceria Nanospheres: Surface Defects Promoted Catalytic Activity and a Versatile Approach. *J. Mater. Chem. A* **2014**, *2*, 5662−5667.
(27) Qin, J.; Lu, J.; Cao, M.; Hu, C. Synthesis of Porous CuO-CeO_2 Nanospheres with an Enhanced Low-Temperature CO Oxidation Activity. *Nanoscale* **2010**, *2*, 2739−2743.
(28) Qi, L.; Yu, Q.; Dai, Y.; Tang, C.; Liu, L.; Zhang, H.; Gao, F.; Dong, L.; Chen, Y. Influence of Cerium Precursors on the Structure and Reducibility of Mesoporous CuO-CeO_2 Catalysts for CO Oxidation. *Appl. Catal., B* **2012**, *119*−*120*, 308−320.
(29) Jia, A. P.; Hu, G. S.; Meng, L.; Xie, Y. L.; Lu, J. Q.; Luo, M. F. CO Oxidation Over CuO/$Ce_{1-x}Cu_xO_{2-\delta}$ and $Ce_{1-x}Cu_xO_{2-\delta}$ Catalysts: Synergetic Effects and Kinetic Study. *J. Catal.* **2012**, *289*, 199−209.
(30) Wang, W. W.; Du, P. P.; Zou, S. H.; He, H. Y.; Wang, R. X.; Jin, Z.; Shi, S.; Huang, Y. Y.; Si, R.; Song, Q. S.; Jia, C. J.; Yan, C. H. Highly Dispersed Copper Oxide Clusters as Active Species in Copper-Ceria Catalyst for Preferential Oxidation of Carbon Monoxide. *ACS Catal.* **2015**, *5*, 2088−2099.
(31) Zeng, S.; Liu, K.; Zhang, L.; Qin, B.; Chen, T.; Yin, Y.; Su, H. Deactivation Analyses of CeO_2/CuO Catalysts in the Preferential Oxidation of Carbon Monoxide. *J. Power Sources* **2014**, *261*, 46−54.
(32) Shen, W. H.; Dong, X. P.; Zhu, Y. F.; Chen, H. R.; Shi, J. L. Mesoporous CeO_2 and CuO-Loaded Mesoporous CeO_2: Synthesis, Characterization, and CO Catalytic Oxidation Property. *Microporous Mesoporous Mater.* **2005**, *85*, 157−162.
(33) Zhou, G.; Lan, H.; Song, R.; Xie, H.; Du, Q. Effects of Preparation Method on CeCu Oxide Catalyst Performance. *RSC Adv.* **2014**, *4*, 50840−50850.
(34) Sun, C.; Sun, J.; Xiao, G.; Zhang, H.; Qiu, X.; Li, H.; Chen, L. Mesoscale Organization of Nearly Monodisperse Flowerlike Ceria Microspheres. *J. Phys. Chem. B* **2006**, *110*, 13445−13452.
(35) Chen, G.; Xu, C.; Song, X.; Zhao, W.; Ding, Y.; Sun, S. Interface Reaction Route to Two Different Kinds of CeO_2 Nanotubes. *Inorg. Chem.* **2008**, *47*, 723−728.
(36) Chen, G.; Rosei, F.; Ma, D. Interfacial Reaction-Directed Synthesis of Ce-Mn Binary Oxide Nanotubes and Their Applications in CO Oxidation and Water Treatment. *Adv. Funct. Mater.* **2012**, *22*, 3914−3920.
(37) Liu, W.; Feng, L.; Zhang, C.; Yang, H.; Guo, J.; Liu, X.; Zhang, X.; Yang, Y. A Facile Hydrothermal Synthesis of 3D Flowerlike CeO_2 Via a Cerium Oxalate Precursor. *J. Mater. Chem. A* **2013**, *1*, 6942−6948.
(38) Chen, G.; Xu, Q.; Wang, Y.; Song, G.; Fan, W. Room Temperature Interfacial Reaction-Directed Synthesis of Hierarchically Porous Ceria from a Water-Soluble Precursor. *J. Mater. Chem. A* **2015**, *3*, 7022−7028.
(39) Chen, G.; Xu, C.; Song, X.; Xu, S.; Ding, Y.; Sun, S. Template-Free Synthesis of Single-Crystalline-Like CeO_2 Hollow Nanocubes. *Cryst. Growth Des.* **2008**, *8*, 4449−4453.
(40) Casari, B. M.; Langer, V. New Structure Type among Octahydrated Rare-Earth Sulfates, β-$Ce_2(SO_4)_3{\cdot}8H_2O$, and A New $Ce_2(SO_4)_3{\cdot}4H_2O$ Polymorph. *Z. Anorg. Allg. Chem.* **2007**, *633*, 1074−1081.

DOI: 10.1021/acsami.5b06495
ACS Appl. Mater. Interfaces 2015, 7, 23538−23544